

## Adsorption of Fe(II) by Layered Double Hydroxide Composite with Carbon-Based Material (Biochar and Graphite): Reusability and Thermodynamic Properties

Neza Rahayu Palapa<sup>1</sup>, Alfian Wijaya<sup>2</sup>, Patimah Mega Syah Bahar Nur Siregar<sup>2</sup>, Amri Amri<sup>2</sup>, Nur Ahmad<sup>2</sup>, Tarmizi Taher<sup>3</sup>, and Aldes Lesbani<sup>2,4\*</sup>

<sup>1</sup>Department of Chemistry, Faculty of Mathematics and Natural Sciences, Sriwijaya University, Jl. Palembang-Prabumulih, Km. 90-32, Ogan Ilir 30862, South Sumatra, Indonesia

<sup>2</sup>Research Center of Inorganic Materials and Complexes, Faculty of Mathematics and Natural Sciences, Sriwijaya University, Jl. Padang Selasa Bukit Besar, Palembang 30139, South Sumatra, Indonesia

<sup>3</sup>Department of Environmental Engineering, Institut Teknologi Sumatera, Jl. Terusan Ryacudu, Way Hui, Lampung Selatan 35365, Indonesia

<sup>4</sup>Graduate School, Faculty of Mathematics and Natural Sciences, Sriwijaya University, Jl. Palembang-Prabumulih, Km. 90-32, Ogan Ilir 30862, South Sumatra, Indonesia

### \* Corresponding author:

email: aldeslesbani@pps.unsri.ac.id

Received: June 10, 2022

Accepted: December 25, 2022

DOI: 10.22146/ijc.75307

**Abstract:** Layered double hydroxide (LDH) of Ni/Al was synthesized by coprecipitation method at pH 10 followed by the formation of composite with carbon-based material i.e., biochar (B) and graphite (G) to form Ni/Al-B and Ni/Al-G. Materials were characterized by XRD powder, FTIR, BET surface area, thermal analyses, and SEM analysis. The regeneration process and adsorption evaluated the performance of materials toward iron(II) [Fe(II)] from an aqueous solution. The results showed that the surface area of Ni/Al-B (428.94 m<sup>2</sup>/g) was increased mainly up to twenty-nine-fold than Ni/Al LDH (15.11 m<sup>2</sup>/g), while Ni/Al-G (21.59 m<sup>2</sup>/g) had slightly increased than pristine LDH. Composite of Ni/Al-B had reusability properties for Fe(II) adsorption up to five cycles and showed higher structural stability. The adsorption capacity of Ni/Al-B was 104.167 mg/g and can be a potential adsorbent to remove Fe(II) from an aqueous solution.

**Keywords:** layered double hydroxide; graphite; biochar; Ni/Al; structural stability

## ■ INTRODUCTION

Adsorption is suitable for removing various wastewater pollutants such as organic molecules, heavy metals, and dyes [1-2]. This method offers several advantages: fast process, easy to conduct, and high efficiency. The successful adsorption process depends on the properties of the adsorbent. The adsorbent can be categorized as inorganic and organic adsorbents [3-5]. Each type of adsorbent has advantages and disadvantages depending on the pollutants and properties of adsorbents [6]. Organic adsorbents such as chitin, chitosan, cellulose, lignin, and algae have various functional groups, which can be used as active sites for the adsorption process [5,7-9]. The organic adsorbents are easily decomposed by temperature. On the other hand, inorganic adsorbents

such as zeolite, clay, metal oxide, bentonite, kaolinite, and layered double hydroxide have pores and layers as active sites for adsorption [10-13]. Inorganic adsorbents are temperature resistant. Based on the advantages and disadvantages of organic-inorganic adsorbents, modification of adsorbents based on organic-inorganic materials is an interesting topic to explore, in regards to obtain novel properties of adsorbents for the removal of pollutants.

Layered double hydroxide (LDH) is an inorganic layered material consisting of divalent and trivalent metal ions with the general formula  $[M^{2+}_x M^{3+}_x (OH)_2]^{x+} (A^{n-})_{x/n} \cdot nH_2O$ , where M is divalent and trivalent metal ions and A<sup>n-</sup> is interlayer anions with valence n [14]. The merit of this material is that it can be

easily modified using various supports by intercalation, impregnation, and support matrix to improve the stability, the interlayer space, and also the thermal/physical properties of the material. LDH is widely used as an adsorbent to remove pollutants from aqueous solution, as reported by Bessaies et al. [15] in which the Ca/Al and Zn/Al LDH have been studied as arsenic removal. The adsorption capacity was obtained at 10.31 and 30.13 mg/g for Ca/Al and Zn/Al LDH, respectively. Rahmadan et al. [16] reported that ZnAl was prepared for the adsorption of cadmium from an aqueous solution and the adsorption capacity was 22.727 mg/g. In another research, LDH was also widely prepared to remove dyes. According to Starukh and Levytska [17], ZnAl LDH was studied for indigo carmine removal at 298 K and obtained an adsorption capacity of 47 mg/g. Mg–Al–Cu–Fe–CO<sub>3</sub> LDH was prepared to remove acid red in adsorption with pH 6.8 at 298 K. The adsorption results showed that the adsorption capacity reached 66.19 mg/g from an initial concentration of 66.1 mg/L. Unfortunately, the adsorption process of LDH still has limitations and has become challenging for researchers. Furthermore, the modification of LDH using several techniques has been explored.

The modification of LDH by intercalation and impregnation is also conducted to increase the interlayer space and stability of materials such as polyoxometalate, organic compounds, and also carbon-based materials. According to Palapa et al. [18], the unique adsorption process of malachite green was obtained by CuAl LDH intercalated using polyoxometalate. The adsorption capacity showed equal data with increasing surface area properties of the material before and after intercalation. The adsorption capacity CuAl LDH intercalated using polyoxometalate is 149.253 mg/g, higher than 55.866 mg/g from CuAl LDH pristine. Siregar et al. [19] showed that the composites of Mg/Al-AH and Mg/Al-HC had a higher adsorption capacity for Cr (VI) (32.017 and 208.333 mg/g, respectively) than pristine Zn/Cr LDHs (30.211 mg/g). Choong et al. [20] had reported the study of polyacrylamide polyvinyl alcohol. LDH results in higher efficiency for As(V) and As(III) removal with maximum adsorption capacities of 22.8 and 14.1 mg/g, respectively,

higher than that of pristine LDH with adsorption capacities of 7.9 and 7.1 mg/g, respectively. Lv et al. [21] also reported that as-prepared ternary (Fe@LDH/rGO) had good efficiency and capacity for Cr(VI) oxyanions. The adsorption capacity increased after modification, from 5.94 to 14.68 mg/g.

Based on the mentioned literature, it is shown that the development of LDH by impregnation to form carbon-based composite is intriguing research. In the current study, LDH Ni/Al will be composited with carbon-based materials i.e., biochar (B) and graphite (G), to form Ni/Al-B and Ni/Al-G composites. B and G are carbon-rich materials and can stabilize the formation of LDH composites. Ni/Al-B and Ni/Al-G composites will be used as adsorbents for iron(II) from an aqueous solution. The reusability of composites will be investigated first to evaluate the structural stability of composites followed by the adsorption thermodynamics of iron(II).

## ■ EXPERIMENTAL SECTION

### Materials

Chemicals such as nickel(II) nitrate, aluminum (III) nitrate, sodium hydroxide, iron(II) nitrate, sodium carbonate, and graphite were supplied from Merck and used directly after being purchased. Biochar was obtained from Bukata Organic Java, Indonesia, by pyrolysis of Indonesian Java rice husk. Water was purified several times by Purite® water resin ion exchange method.

### Instrumentation

Characterization of materials was performed by powder XRD Rigaku Miniflex-600 by scanning at 1°/min. Functional groups were analyzed by FTIR Shimadzu Prestige-21 using the KBr method. BET analysis was conducted using Quantachrome Micrometric 2020, and the sample was degassed under liquid N<sub>2</sub> prior to analysis. Thermal analysis was conducted using TG-DTA Shimadzu analyzer using N<sub>2</sub> flow. SEM analysis was conducted using Scanning Electron Microscopes (SEM) analyzer SU800 Series. The concentration of Fe(II) was analyzed by UV-Visible Bio-

Base BK-UV 1800 PC spectrophotometer after complexation using 1,10-phenanthroline as a ligand at 510 nm.

## Procedure

### Synthesis of Ni/Al LDH

Ni/Al LDH was synthesized by the coprecipitation method at pH 10. As much as 100 mL of nickel(II) nitrate and aluminum(III) nitrate mixture was made with a concentration ratio of 3:1. The mixture was constantly stirred at room temperature, and sodium carbonate (0.3 M) was added. The pH mixture was adjusted to 10 by the addition of sodium hydroxide solution. The reaction was kept at 80 °C for 24 h. The solid material was filtered, washed and dried at 110 °C.

### Preparation of Ni/Al-G and Ni/Al-B

Preparation of Ni/Al-G and Ni/Al-B was conducted by the coprecipitation method. As much as 100 mL of nickel(II) nitrate and aluminum(III) nitrate mixture with the concentration ratio molar of 3:1 was stirred for 60 min. G was added to the mixture by constant stirring followed by the addition of sodium hydroxide (2 M). The pH of the mixture was adjusted with a solution of sodium hydroxide up to pH 10. The reaction mixture was constantly stirred for 72 h. The solid material of Ni/Al-G was formed, washed, and dried at 110 °C for 3 days. The preparation of Ni/Al-B was similar to Ni/Al-G but by changing G to B to form Ni/Al-B.

### Structural stability of materials toward re-adsorption

Structural stability of Ni/Al-G, Ni/Al-B, Ni/Al LDH, G, and B was evaluated by Fe(II) re-adsorption process after desorption using an ultrasonic system. After Fe(II) adsorption, the adsorbent was desorbed by an ultrasonic system equipped with a water chamber and then the adsorbent was dried at 110 °C for 3 h. The adsorbent was then reused for Fe(II) adsorption. Re-adsorption was performed until five cycles.

### Adsorption isotherm

Adsorption of Fe(II) on composite and pristine materials was conducted by the batch system. Adsorption isotherm was studied by variation of the Fe(II) initial concentration and temperature. The concentration of Fe(II) was adjusted to 10, 20, 30, 40, and 50 mg/L and

adsorption temperature was set to 30, 40, 50, and 60 °C. The concentration of Fe(II) after adsorption on the filtrate was analyzed at 510 nm using a UV-Visible spectrophotometer.

## RESULTS AND DISCUSSION

The XRD powder patterns of the composite based on B and G and also the pristine materials are presented in Fig. 1. Ni/Al LDH had diffraction patterns at 11.63° (003); 23.00° (006); 35.16° (012); 39.56° (015); 47.4° (018) and 61.59° (110) [22]. These patterns show the formation of well-known layer structures at 11.63° (003) and 61.59° (110). The diffraction pattern of Ni/Al LDH shows the high crystallinity of the material, which was different from B, as shown in Fig. 1(b). B had a broad diffraction pattern and had one maximum diffraction peak at around 22.30° (002). The diffraction at (002) was attributed to the high carbon content of B from rice husk [23]. On the other hand, the diffraction peak of G was one sharp peak at 26.5° (002) and one small peak at 54° (004). These diffraction peaks were reflected from polyarene structures [24]. The formation of composite based on the carbon material i.e., Ni/Al-B and Ni/Al-G, is shown in Fig. 1(d) and 1(e). Ni/Al-B had a broad diffraction peak, which was similar to B at 22.3° (002). Other diffraction peaks were detected at 11.63° (003) and 36° (012) that come from Ni/Al LDH. Thus, the formation of the composite was based on the starting

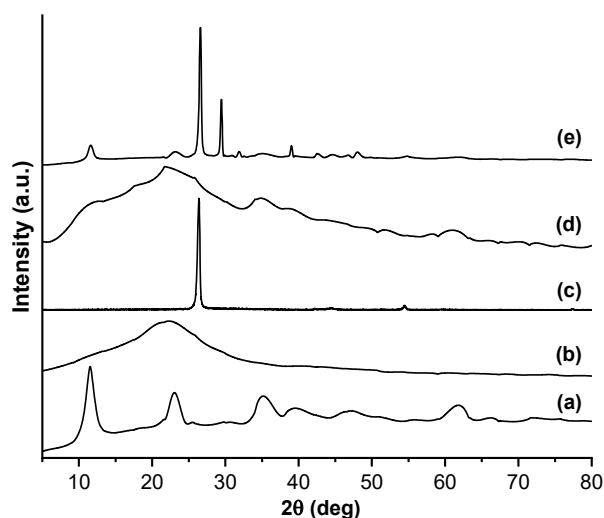


Fig 1. XRD patterns of Ni/AL LDH (a), B (b), G (c), Ni/Al-B (d), and Ni/Al-G (e)

materials. These phenomena were also found for the composite based on G. Ni/Al-G had higher crystallinity than Ni/Al-B. The diffraction of Ni/Al-G was detected at  $11.63^\circ$ ,  $26.5^\circ$  (middle intensity),  $29^\circ$  (high intensity), and low intensity at  $32^\circ$ ,  $41^\circ$ ,  $44^\circ$  and  $48^\circ$ . All diffractions were contributed to LDH and G. Thus, the formation of a composite based on carbon materials was successfully conducted.

The functional groups of the composite and pristine materials were detected by FTIR spectra, as shown in Fig. 2. Ni/Al LDH had main vibration peaks at  $3448\text{ cm}^{-1}$  ( $\nu$  O-H stretching),  $1635\text{ cm}^{-1}$  ( $\nu$  O-H bending), and  $1381\text{ cm}^{-1}$  ( $\nu$  N-O, nitrate, stretching). B had an organic compound and the main vibration appeared at  $3448\text{ cm}^{-1}$  ( $\nu$  O-H stretching),  $1635\text{ cm}^{-1}$  ( $\nu$  O-H bending, and  $1095\text{ cm}^{-1}$  ( $\nu$  C-O stretching). The C-H vibration was also found at  $2368\text{ cm}^{-1}$  on B. Similar vibration with B was detected on G at  $3448$ ,  $2368$ ,  $1635$ , and  $1381\text{ cm}^{-1}$  [25]. Composites Ni/Al-B and Ni/Al-G consisted of LDH, B, and G thus, all vibrations of LDH-B and LDH-G should have appeared with almost similar vibrations, as shown in Fig. 2(d) and 2(e).

The nitrogen isotherm adsorption-desorption of composite and starting materials is shown in Fig. 3. All materials have a hysteresis loop due to the adsorption step being different from the desorption step. The materials also had type IV adsorption-desorption curves in which the distribution size of the materials was ununiform [26]. Mesoporous size type was mixed with microporous size in this case. The data of the adsorption-desorption isotherm in Fig. 3 was then calculated using Brunauer-Emmett-Teller (BET) method to obtain the value of the surface area, pore size, and pore distribution, as shown in Table 1.

The BET data in Table 1 shows that Ni/Al-B had a

higher surface area properties compared to the Ni/Al-G composite. The increased surface area properties of Ni/Al-B are almost twenty-nine-fold that of Ni/Al LDH.

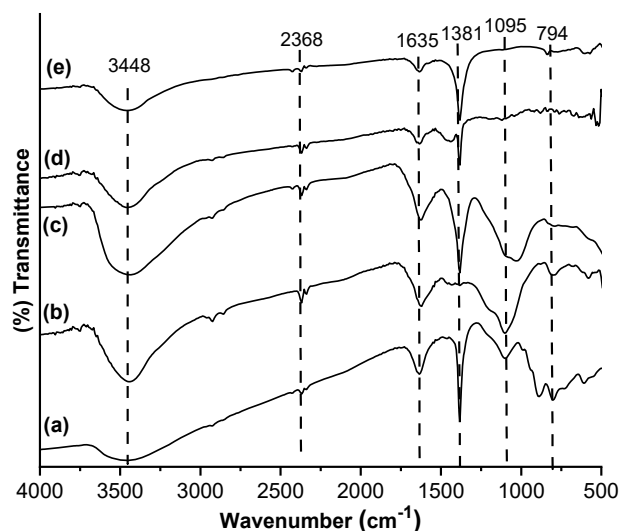


Fig 2. FTIR spectrum of Ni/Al LDH (a), B (b), G (c), Ni/Al-B (d), and Ni/Al-G (e)

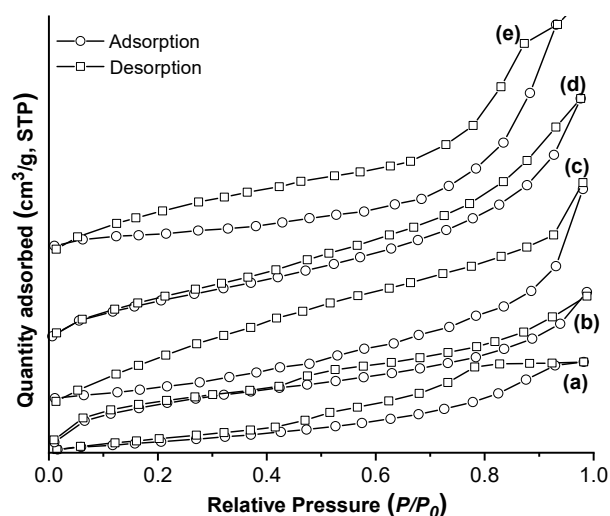


Fig 3. N<sub>2</sub> adsorption-desorption profile of Ni/Al LDH (a), B (b), G (c), Ni/Al-B (d), and Ni/Al-G (e)

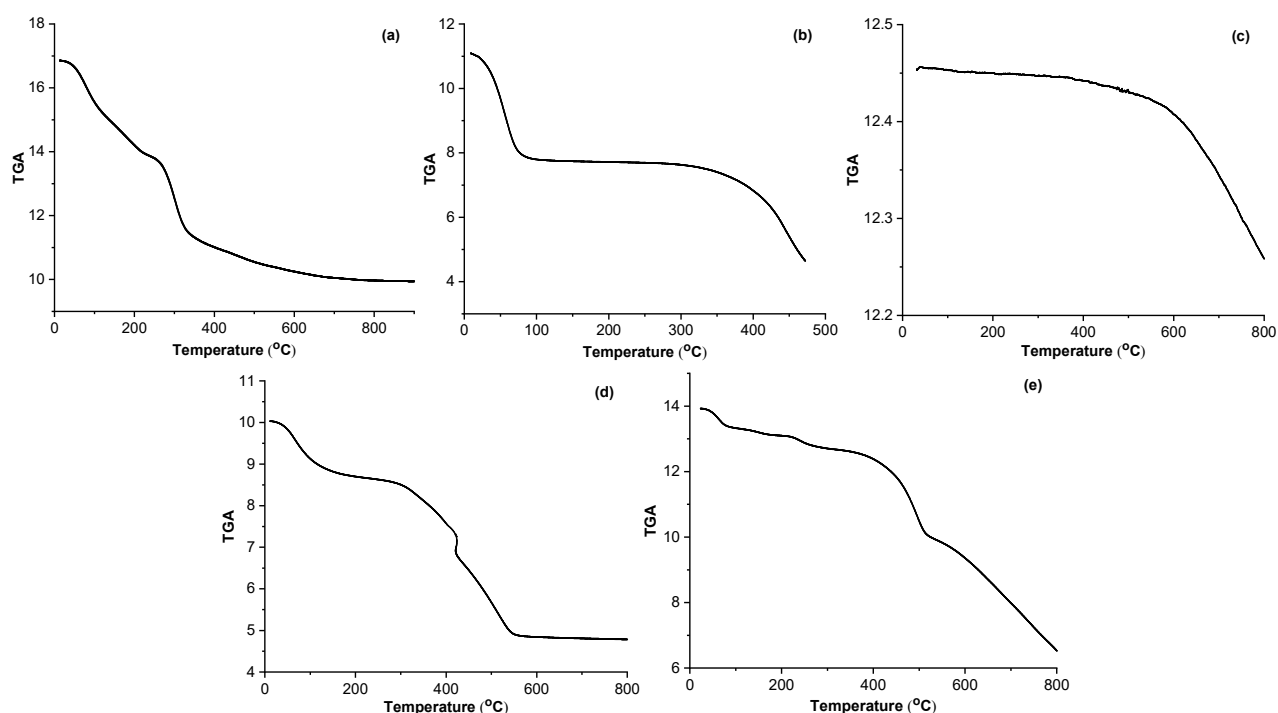
Table 1. BET data of materials

Materials	Surface area (m <sup>2</sup> /g)	Pore size (nm), BJH	Pore volume (cm <sup>3</sup> /g) <sub>BJH</sub>
Ni/Al LDH	15.11	2.90	0.04
B	50.94	12.09	0.02
G	11.56	3.17	0.03
Ni/Al-B	438.94	12.30	0.002
Ni/Al-G	21.59	3.15	0.03

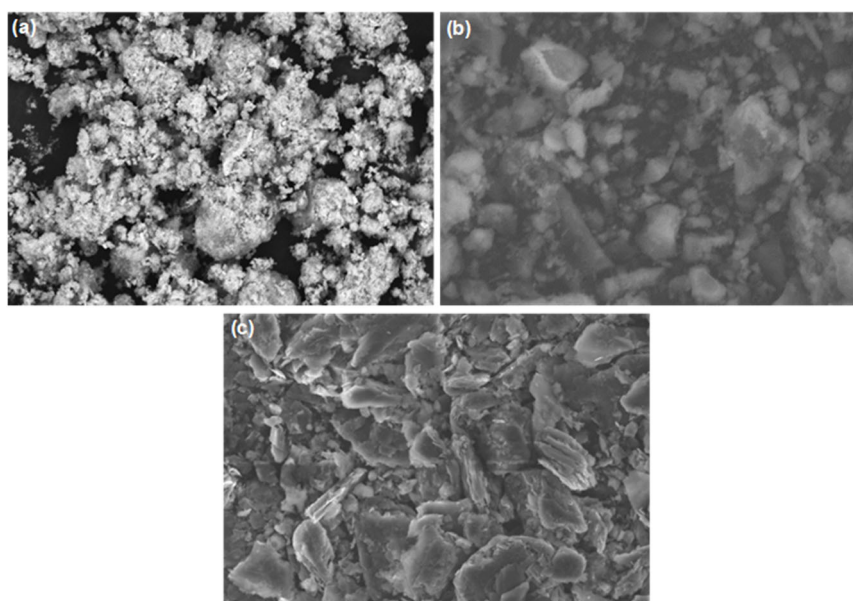
On the other hand, the surface area and pore size of Ni/Al-G were slightly higher than Ni/Al-B. The lower surface area of Ni/Al-G compared to Ni/Al-G was because G covered the surface sites of LDH by polyarene. The active site of Ni/Al-G was dominated by G, which was collated with a composite of high crystallinity, similar to G.

Fig. 4 shows the thermal properties of the

composites and starting materials. Ni/Al LDH is an inorganic layer material that had three endothermic peaks, as shown in Fig. 4(a). The endothermic peaks were identified at 100 °C (loss of water on surface material), 220 °C (loss of water of crystallization), and 320 °C (decomposition of anion on the interlayer). On the other hand, B, which is an organic material had one



**Fig 4.** TGA profile of Ni/Al LDH (a), B (b), G (c), Ni/Al-B (d), and Ni/Al-G (e)



**Fig 5.** SEM images of Ni/Al LDH (a), Ni/Al-B (b), and Ni/Al-G

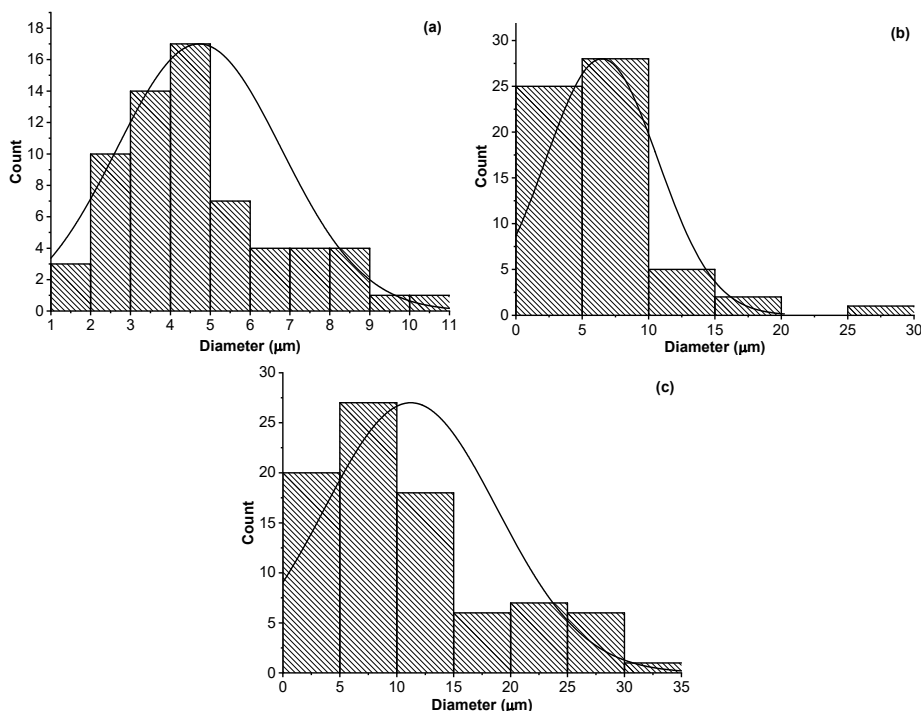


**Fig 6.** The particle size of Ni/Al LDH (a), Ni/Al-B (b), and Ni/Al-G (c)

endothermic peak and one exothermic peak. The endothermic peak at 95 °C was attributed to the loss of water on surface B. The exothermic peak at 490 °C was identified as the oxidation of an organic compound on B. The G material had one endothermic peak at 795 °C due to the decomposition of the G layer [27]. Composites Ni/Al-B and Ni/Al-G had both endothermic and exothermic peaks, which was related to the decomposition of inorganic substances and oxidation of organic molecules on the composite, as shown in Fig. 4(d) and 4(e).

The SEM images and particle size of Ni/Al LDH, Ni/Al-B, and Ni/Al-G are shown in Fig. 5 and 6. Based on Fig. 5, it is indicated that the morphology of Ni/Al LDH, Ni/Al-B, and Ni/Al-G materials form aggregates and tends to be heterogeneous. From the data of particle sizes in Fig. 6, it can be seen that the mean particle size of Ni/Al LDH, Ni/Al-B, and Ni/Al-G are 4.787, 6.568, and 11.328 μm, respectively.

To evaluate the ability of a composite as an adsorbent with high stability structure toward the adsorption of Fe(II), the regeneration and re-adsorption of the adsorbent was performed until five cycles as shown in Fig. 7. FTIR analysis was carried out on the adsorbent

after the re-adsorption process (Fig. 8) which showed no change in the material structure characterized by insignificant wavenumber shifts and vibrations that appeared the same as the initial material.

The composite of Ni/Al-B had a higher adsorption capacity than Ni/Al-G. As mentioned in the previous results, the surface area of Ni/Al-B was higher than Ni/Al-G and Ni/Al LDH, thus giving the highest adsorption

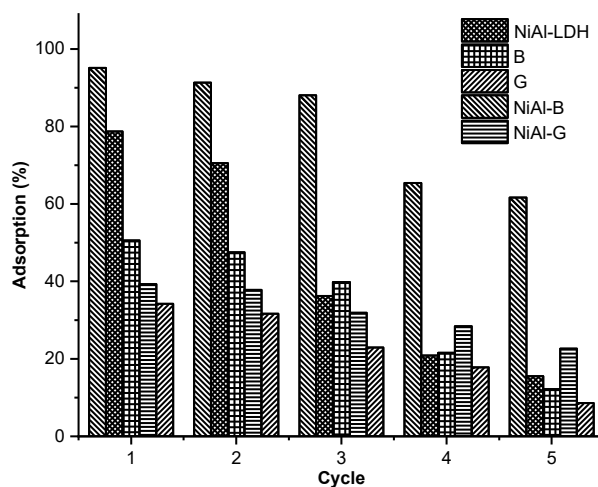


**Fig 7.** Reusability of adsorbent until five cycles re-adsorption process

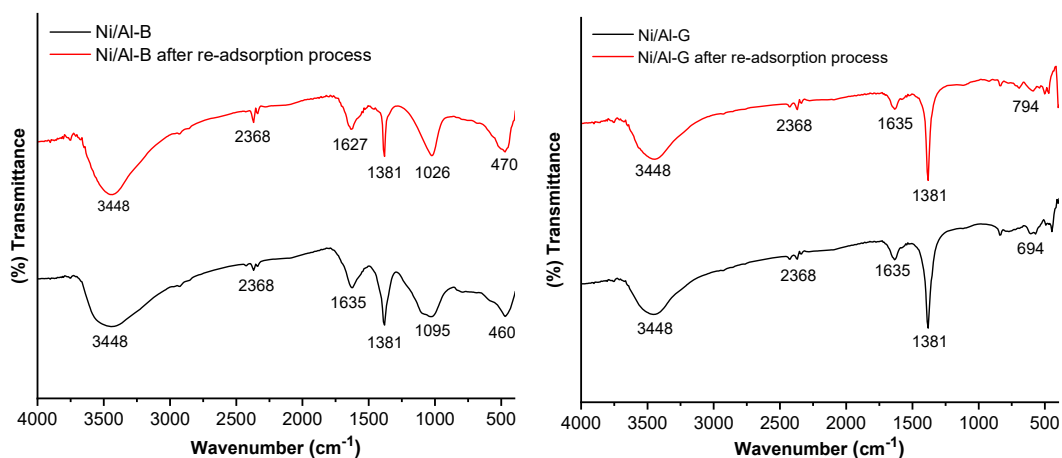
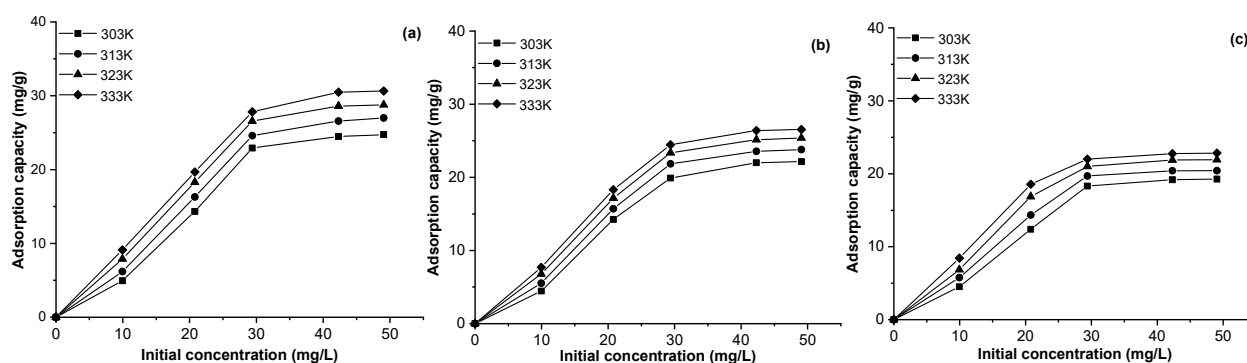


Fig 8. FTIR spectrum of Ni/Al-B and Ni/Al-G after the re-adsorption process

capacity toward Fe(II). Adsorption of Fe(II) on B was higher than on G. The reusability of the Ni/Al-B adsorbent until five re-adsorption processes gave a relatively stable structure toward Fe(II) adsorption compared to the other adsorbents. The Fe(II) adsorption on Ni/Al-B at five re-adsorption processes reached more than 70%. These phenomena showed that the active site of Ni/Al-B was relatively retained, although it had adsorption-desorption cycles [27-28]. The composite of Ni/Al-G also showed similar phenomena to Ni/Al-B. Although the adsorption capacity of Fe(II) in Ni/Al-G is low, the re-adsorption process resulted in almost the same adsorption capacity, in the range of 39–32%, up to five cycles. The pristine material of Ni/Al LDH had decreasing adsorption capacity at the third re-adsorption cycle due to the exfoliation of the LDH structure. The adsorption capacity of B and G was also decreased sharply due to unstable organic materials toward the desorption process. Thus, the formation of composite by carbon-based materials can increase the structural stability of Ni/Al LDH.

Adsorption of Fe(II) on the aqueous solution by pristine materials and composites is shown in Fig. 9. Adsorption of Fe(II) gradually increased by increasing the Fe(II) initial concentration and reached equilibrium at almost 40 mg/L for all adsorbents. Adsorption of Fe(II) was increased with increasing adsorption temperature from 303 K to 333 K. The data in Fig. 9 was then calculated using Langmuir and Freundlich isotherm models to obtain the adsorption isotherm model of Fe(II). Furthermore, the adsorption thermodynamic was obtained by the calculation of  $\Delta H$ ,  $\Delta G$ , and  $\Delta S$ . The isotherm data and adsorption thermodynamics are presented in Tables 2 and 3.

Adsorption isotherm Langmuir and Freundlich models were applied to obtain adsorption isotherm of Fe(II) on composites and starting materials. The isotherm for each adsorbent followed different types of models. Starting materials of G, B, and Ni/Al LDH almost follows the Langmuir model more than the Freundlich model. Layered materials such as Ni/AL LDH



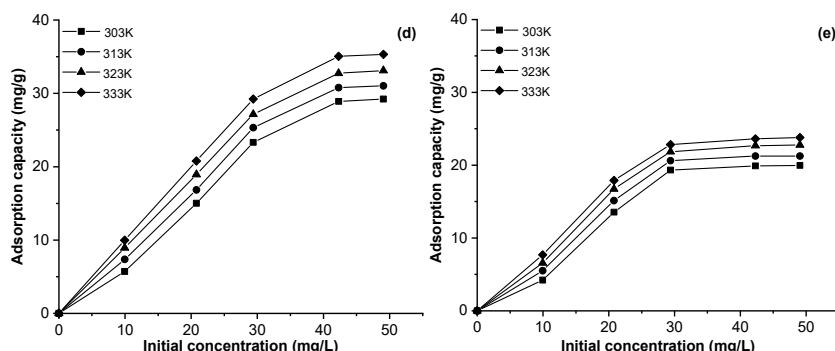


**Fig 9.** Effect of Fe(II) adsorption by variation of Fe(II) initial concentration and temperature on Ni/Al LDH (a), B (b), G (c), Ni/Al-B (d), and Ni/Al-G (e)

**Table 2.** Isotherm model for Fe(II) adsorption on LDH, B, G, and composites

Adsorbent	Adsorption isotherm	Adsorption constant	T (K)			
			303	313	323	333
G	Langmuir	$Q_{\max}$	22.936	20.523	22.936	23.310
		$k_L$	0.199	0.387	0.906	1.977
		$R^2$	0.9678	0.9913	0.9993	0.999
	Freundlich	$n$	0.498	27.855	25.575	32.468
		$k_F$	6.411	18.180	19.355	20.711
		$R^2$	0.9849	0.9538	0.9616	0.9809
B	Langmuir	$Q_{\max}$	25.974	26.455	27.248	31.250
		$k_L$	0.241	0.393	0.633	0.295
		$R^2$	0.9869	0.993	0.9974	0.9436
	Freundlich	$n$	0.148	1.2	1.647	2.398
		$k_F$	2.718	4.061	7.852	12.578
		$R^2$	0.999	0.999	0.999	0.999
Ni/Al LDH	Langmuir	$Q_{\max}$	29.412	27.701	30.395	31.447
		$k_L$	0.999	1.597	0.997	2.356
		$R^2$	0.9486	0.999	0.9964	0.9995
	Freundlich	$n$	16.949	0.174	0.225	24.272
		$k_F$	20.554	3.284	2.116	2.734
		$R^2$	0.9906	0.9993	0.9934	0.9845
Ni/Al-G	Langmuir	$Q_{\max}$	42.373	31.056	28.653	26.954
		$k_L$	0.138	0.366	0.650	1.111
		$R^2$	0.9618	0.9997	0.9983	0.970
	Freundlich	$n$	31.250	35.587	28.902	31.746
		$k_F$	17.968	19.422	20.384	21.513
		$R^2$	0.9762	0.9465	0.9834	0.9959
Ni/Al-B	Langmuir	$Q_{\max}$	104.167	48.309	42.017	42.017
		$k_L$	0.137	0.593	1.478	1.831
		$R^2$	0.997	0.725	0.932	0.999
	Freundlich	$n$	0.275	0.413	0.723	2.257
		$k_F$	1.422	1.382	1.239	1.035
		$R^2$	0.9663	0.9276	0.9907	0.9905

**Table 3.** Adsorption thermodynamic of Fe(II) on LDH, B, G, and composites

Adsorbents	T (K)	Q <sub>e</sub> (mg/g)	ΔH (kJ/mol)	ΔS (kJ/mol)	ΔG (kJ/mol)
G	303	19.268	9.056	0.035	-1.408
	313	20.428			-1.753
	323	21.929			-2.099
	333	22.849			-2.444
B	303	22.149	1.022	0.032	-8.666
	313	23.79			-8.985
	323	25.39			-9.305
	333	26.551			-9.625
Ni/Al LDH	303	24.730	13.562	0.045	-0.052
	313	26.991			-0.501
	323	28.772			-0.950
	333	30.643			-1.400
Ni/Al-G	303	19.968	9.449	0.036	-1.561
	313	21.248			-1.924
	323	22.769			-2.288
	333	23.790			-2.651
Ni/Al-B	303	29.218	13.943	0.049	-0.958
	313	31.027			-1.450
	323	33.108			-1.942
	333	35.317			-2.433

**Table 4.** Comparison of Fe(II) adsorption capacity on several adsorbents

Adsorbent	Adsorbate	Adsorption capacity (mg/g)	Reference
Co/Mo LDH	Fe(II)	10	[31]
Ca/Al LDH		11.16	[32]
Zn/Cr-POM		76.923	[19]
Banana peel		33.79	[33]
Intercalated Ca/Al LDH		11.93	[32]
Bentonite		7.09	[34]
Chitosan		64.10	[35]
Sawdust		6.54	[36]
Rice husk ask		6.211	[37]
Pomegranate peel carbon		18.52	[38]
Zn/Cr LDH		50	[19]
Intercalated Co/Mo LDH with carbonate		77.9	[39]
Ni/Al LDH intercalated with keggion ion		36.496	[22]
Rice husk ask			
Ni/Al LDH		31.447	This Work
B		31.250	This Work
G		23.310	This Work
Ni/Al-B		104.167	This Work
Ni/Al-G		42.373	This Work

and G follow the Langmuir isotherm model, while B follows the Freundlich model. On the other hand, Ni/Al-G and Ni/Al-B follow Freundlich and Langmuir isotherm models, where the R-value was close to one [29]. Adsorption temperature gave an effect on the isotherm of Fe(II) on composites such as Ni/Al-G at low temperatures following the Langmuir isotherm model, but Ni/Al-B follows the Freundlich isotherm model. The adsorption thermodynamic of Fe(II) on composites and starting materials shows negative  $\Delta G$  for all temperature adsorption due to the spontaneity of the adsorption process. The negative value of  $\Delta G$  increased by increasing the temperature. The opposite result was found for  $\Delta S$ , which had a positive value due to growing randomness of the adsorption process between adsorbent and adsorbate.

The value of  $\Delta H$  was also positive. The value of  $\Delta H$  for G, B, and Ni/Al LDH was 9.056–43.540, 1.022–40.655, and 13.562–54.939 kJ/mol, respectively. On the other hand, the value of  $\Delta H$  for composites was higher than the starting materials namely in the range of 9.449–75.800 kJ/mol. All value of  $\Delta H$  was less than 100 kJ/mol, and that was categorized as physical adsorption [30]. Although the involvement of chemical interaction occurred in the adsorption, their contribution was low. Thus adsorption of Fe(II) on the starting materials and composite was classified as physical adsorption.

Table 4 shows that various adsorbents had been tested to remove Fe(II) from an aqueous solution ranging from organic to inorganic adsorbents. The composite of Ni/Al-B in this research shows the highest adsorption capacity among the other adsorbents. On the other hand, Ni/Al-G had a middle adsorption capacity, only up to 42.373 mg/g and slightly higher than the starting materials. Thus Ni/Al-B was a potential composite for the removal of Fe(II) from an aqueous solution.

## ■ CONCLUSION

Composites Ni/Al-G and Ni/Al-B were successfully prepared and had different adsorption properties toward Fe(II) on the aqueous solution. The surface area of Ni/Al-B (438.942 m<sup>2</sup>/g) was largely higher than Ni/Al-G (21.595 m<sup>2</sup>/g). Adsorption of Fe(II) on the composite was higher than on the starting material. The adsorption

capacity of Ni/Al-G and Ni/Al-B was up to 42.373 and 104.167 mg/g, respectively. The adsorption energy was less than 100 kJ/mol for both starting materials, and composites indicated that the adsorption of Fe(II) on G, B, Ni/Al LDH, Ni/Al-G, and Ni/Al-B was physical adsorption. Ni/Al-B can be reused up to five cycles of re-adsorption and shows the structural stability toward the adsorption of Fe(II).

## ■ ACKNOWLEDGMENTS

The authors thank the Research Center of Inorganic Materials and Coordination Complexes FMIPA Universitas Sriwijaya for instrumental and lab analysis.

## ■ REFERENCES

- [1] Zubair, M., Daud, M., McKay, G., Shehzad, F., and Al-Harhi, M.A., 2017, Recent progress in layered double hydroxides (LDH)-containing hybrids as adsorbents for water remediation, *Appl. Clay Sci.*, 143, 279–292.
- [2] Esan, O.S., Kolawole, A.O., and Olumuyiwa, A.C., 2019, The removal of single and binary basic dyes from synthetic wastewater using bentonite clay adsorbent, *Am. J. Polym. Sci. Technol.*, 5 (1), 16–28.
- [3] Ouassif, H., Moujahid, E.M., Lahkale, R., Sadik, R., Bouragba, F.Z., Sabbar, E., and Diouri, M., 2020, Zinc-aluminum layered double hydroxide: High efficient removal by adsorption of tartrazine dye from aqueous solution. *Surf. Interfaces*, 18, 100401.
- [4] Jitianu, M., Gunness, D.C., Aboagye, D.E., Zaharescu, M., and Jitianu, A., 2013, Nanosized Ni–Al layered double hydroxides—Structural characterization, *Mater. Res. Bull.*, 48 (5), 1864–1873.
- [5] Cheng, S.Y., Show, P.L., Lau, B.F., Chang, J.S., and Ling, T.C., 2019, New prospects for modified algae in heavy metal adsorption, *Trends Biotechnol.*, 37 (11), 1255–1268.
- [6] Yagub, M.T., Sen, T.K., Afroze, S., and Ang, H.M., 2014, Dye and its removal from aqueous solution by adsorption: A review, *Adv. Colloid Interface Sci.*, 209, 172–184.

- [7] Boulaiche, W., Hamdi, B., and Trari, M., 2019, Removal of heavy metals by chitin: Equilibrium, kinetic and thermodynamic studies, *Appl. Water Sci.*, 9 (2), 39.
- [8] Okon, A.N., Udoh, F.D., and Bassey, P.G., 2014, Evaluation of Rice Husk as Fluid Loss Control Additive in Water-Based Drilling Mud, *SPE Nigeria Annual International Conference and Exhibition*, August 5–7, 2014, Lagos, Nigeria.
- [9] Patil, N.P., Bholay, A.D., Kapadnis, B.P., and Gaikwad, V.B., 2016, Biodegradation of model azo dye methyl red and other textile dyes by isolate *Bacillus circulans* NPP1, *J. Pure Appl. Microbiol.*, 10 (4), 2793–2800.
- [10] Vimonses, V., Lei, S., Jin, B., Chow, C.W.K., and Saint, C., 2009, Kinetic study and equilibrium isotherm analysis of Congo Red adsorption by clay materials, *Chem. Eng. J.*, 148 (2-3), 354–364.
- [11] Ravi, R., and Pandey, L.M., 2019, Enhanced adsorption capacity of designed bentonite and alginate beads for the effective removal of methylene blue, *Appl. Clay Sci.*, 169, 102–111.
- [12] Taher, T., Rohendi, D., Mohadi, R., and Lesbani, A., 2019, Congo red dye removal from aqueous solution by acid-activated bentonite from sarolangun: kinetic, equilibrium, and thermodynamic studies, *Arab J. Basic Appl. Sci.*, 26 (1), 125–136.
- [13] Palapa, N.R., Taher, T., Rahayu, B.R., Mohadi, R., Rachmat, A., and Lesbani, A., 2020, CuAl LDH/rice husk biochar composite for enhanced adsorptive removal of cationic dye from aqueous solution, *Bull. Chem. React. Eng. Catal.*, 15 (2), 525–537.
- [14] Chakraborty, C., Dana, K., and Malik, S., 2011, Intercalation of perylenediimide dye into LDH clays: Enhancement of photostability, *J. Phys. Chem. C*, 115 (5), 1996–2004.
- [15] Bessaies, H., Iftekhar, S., Doshi, B., Kheriji, J., Ncibi, M.C., Srivastava, V., Sillanpää, M., and Hamrouni, B., 2020, Synthesis of novel adsorbent by intercalation of biopolymer in LDH for the Removal of arsenic from synthetic and natural water, *J. Environ. Sci.*, 91, 246–261.
- [16] Rahmadan, J., Parhusip, V., Palapa, N.R., Taher, T., Mohadi, R., and Lesbani, A., 2021, ZnAl-humic acid composite as adsorbent of cadmium(II) from aqueous solution, *Sci. Technol. Indones.*, 6 (4), 247–255.
- [17] Starukh, H., and Levytska, S., 2019, The simultaneous anionic and cationic dyes removal with Zn–Al layered double hydroxides, *Appl. Clay Sci.*, 180, 105183.
- [18] Palapa, N.R., Juleanti, N., Normah, N., Taher, T., and Lesbani, A., 2020, Unique adsorption properties of malachite green on interlayer space of Cu-Al and Cu-Al-SiW<sub>12</sub>O<sub>40</sub> layered double hydroxides, *Bull. Chem. React. Eng. Catal.*, 15 (3), 653–661.
- [19] Siregar, P.M.S.B.N., Wijaya, A., Amri, A., Nduru, J.P., Hidayati, N., Lesbani, A., and Mohadi, R., 2022, Layered double hydroxide/C (C=humic acid;hydrochar) as adsorbents of Cr(VI), *Sci. Technol. Indones.*, 7 (1), 41–48.
- [20] Choong, C.E., Wong, K.T., Jang, S.B., Saravanan, P., Park, C., Kim, S.H., Jeon, B.H., Choi, J., Yoon, Y., and Jang, M., 2021, Granular Mg-Fe layered double hydroxide prepared using dual polymers: Insights into synergistic removal of As(III) and As(V), *J. Hazard. Mater.*, 403, 123883.
- [21] Lv, X., Qin, X., Wang, K., Peng, Y., Wang, P., and Jiang, G., 2019, Nanoscale zero valent iron supported on MgAl-LDH-decorated reduced graphene oxide: Enhanced performance in Cr(VI) removal, mechanism and regeneration, *J. Hazard. Mater.*, 373 (6), 176–186.
- [22] Lesbani, A., Normah, N., Palapa, N.R., Taher, T., Andreas, R., and Mohadi, R., 2020, Removal of iron(II) using Ni/Al layered double hydroxide intercalated with Keggin ion, *Molekul*, 15 (3), 149–157.
- [23] Palapa, N.R., Juleanti, N., Mohadi, R., Taher, T., and Rachmat, A., 2020, Copper aluminum layered double hydroxide modified by biochar and its application as an adsorbent for procion red, *J. Water Environ. Technol.*, 18 (6), 359–371.

- [24] Zhu, X., Liu, Y., Qian, F., Zhou, C., Zhang, S., and Chen, J., 2014, Preparation of magnetic porous carbon from waste hydrochar by simultaneous activation and magnetization for tetracycline removal, *Bioresour. Technol.*, 154, 209–214.
- [25] Li, R., Wang, J.J., Zhou, B., Awasthi, M.K., Ali, A., Zhang, Z., Gaston, L.A., Lahori, A.H., and Mahar, A., 2016, Enhancing phosphate adsorption by Mg/Al layered double hydroxide functionalized biochar with different Mg/Al ratios, *Sci. Total Environ.*, 559, 121–129.
- [26] Modwi, A., Abbo, M.A., Hassan, E.A., Al-Duaij, O.K., and Houas, A., 2017, Adsorption kinetics and photocatalytic degradation of malachite green (MG) via Cu/ZnO nanocomposites, *J. Environ. Chem. Eng.*, 5 (6), 5954–5960.
- [27] Luo, X., Wang, C., Wang, L., Deng, F., Luo, S., Tu, X., and Au, C., 2013, Nanocomposites of graphene oxide-hydrated zirconium oxide for simultaneous removal of As(III) and As(V) from water, *Chem. Eng. J.*, 220, 98–106.
- [28] Ribas, M.C., de Franco, M.A.E., Adebayo, M.A., Lima, E.C., Parkes, G.M.B., and Feris, L.A., 2020, Adsorption of Procion Red MX-5B dye from aqueous solution using homemade peach and commercial activated carbons, *Appl. Water Sci.*, 10 (6), 154.
- [29] Hu, F., Wang, M., Peng, X., Qiu, F., Zhang, T., Dai, H., Liu, Z., and Cao, Z., 2018, High-efficient adsorption of phosphates from water by hierarchical CuAl/biomass carbon fiber layered double hydroxide, *Colloids Surf., A*, 555, 314–323.
- [30] Sharifpour, E., Alipanahpour Dil, E., Asfaram, A., Ghaedi, M., and Goudarzi, A., 2019, Optimizing adsorptive removal of malachite green and methyl orange dyes from simulated wastewater by Mn-doped CuO-nanoparticles loaded on activated carbon using CCD-RSM: Mechanism, regeneration, isotherm, kinetic, and thermodynamic studies, *Appl. Organomet. Chem.*, 33 (3), e4768.
- [31] Mostafa, M.S., Bakr, A.A., Eshaq, G., and Kamel, M.M., 2015, Novel Co/Mo layered double hydroxide: Synthesis and uptake of Fe(II) from aqueous solutions (Part 1), *Desalin. Water Treat.*, 56 (1), 239–247.
- [32] Taher, T., Christina, M.M., Said, M., Hidayati, N., Ferlinahayati, F., and Lesbani, A., 2019, Removal of iron(II) using intercalated Ca/Al layered double hydroxides with  $[\alpha\text{-SiW}_{12}\text{O}_{40}]^{4-}$ , *Bull. Chem. React. Eng. Catal.*, 14 (2), 260–267.
- [33] Shrestha, S.L., 2018, Study of the adsorption kinetics of iron ion from wastewater using banana peel, *Int. J. Adv. Res. Chem. Sci.*, 5 (3), 1–8.
- [34] Ain, Q.U., Zhang, H., Yaseen, M., Rasheed, U., Liu, K., Subhan, S., and Tong, Z., 2020, Facile fabrication of hydroxyapatite-magnetite-bentonite composite for efficient adsorption of Pb(II), Cd(II), and crystal violet from aqueous solution, *J. Cleaner Prod.*, 247, 119088.
- [35] Wan Ngah, W.S., Ab Ghani, S., and Kamari, A., 2005, Adsorption behaviour of Fe(II) and Fe(III) ions in aqueous solution on chitosan and cross-linked chitosan beads, *Bioresour. Technol.*, 96 (4), 443–450.
- [36] El-Sherif, I.Y., Fathy, N.A., and Hanna, A.A., 2013, Removal of Mn(II) and Fe(II) ions from aqueous solution using precipitation and adsorption methods, *J. Appl. Sci. Res.*, 9 (1), 233–239.
- [37] Zhang, Y., Zhao, J., Jiang, Z., Shan, D., and Lu, Y., 2014, Biosorption of Fe(II) and Mn(II) ions from aqueous solution by rice husk ash, *Biomed Res. Int.*, 2014, 973095.
- [38] Moghadam, M.R., Nasirizadeh, N., Dashti, Z., and Babanezhad, E., 2013, Removal of Fe(II) from aqueous solution using pomegranate peel carbon: Equilibrium and kinetic studies, *Int. J. Ind. Chem.*, 4 (1), 19.
- [39] Bakr, A.A., Mostafa, M.S., Eshaq, G., and Kamel, M.M., 2015, Kinetics of uptake of Fe(II) from aqueous solutions by Co/Mo layered double hydroxide (Part 2), *Desalin. Water Treat.*, 56 (1), 248–255.